Cavity Ringdown Spectrum of the $T_1(n,\pi^*) \leftarrow S_0$ Transition of 4-Cyclopentene-1,3-dione†

Mitchell G. Springer, Nikolaus C. Hlavacek, Sydney P. Jagusch, Andrew R. Johnson, and Stephen Drucker*

Department of Chemistry, University of Wisconsin—Eau Claire, Eau Claire, Wisconsin 54701-4004

Received: May 4, 2009; Revised Manuscript Received: July 21, 2009

The cavity ringdown absorption spectrum of 4-cyclopentene-1,3-dione was recorded near 487 nm in a room-temperature gas cell. The very weak band system ($\varepsilon \approx 0.05$ dm^3 mol^{-1} cm^{-1}) in this region is due to the $T_1(n,\pi^*) \leftarrow S_0$ electronic transition. The origin-band maximum was observed at 20 540.0 ± 0.5 cm^{-1}. We have assigned about 40 vibronically resolved bands in a region extending to +1100 cm^{-1} relative to the origin. Assignments were aided by quantum-chemical calculations of the $T_1 \leftarrow S_0$ 0−0 excitation energy as well as ground-state vibrational frequencies. From the CRD spectral assignments, we determined fundamental frequencies for several vibrational modes in the T_1 excited state, including the lowest-energy ring-bending and -twisting modes, ν'_{19} (b_1) and ν'_{14} (a_2), respectively. Their fundamentals in the T_1 state are 160.5 and 246 cm^{-1}, compared to 99 and 239 cm^{-1}, respectively, in the S_0 ground state. The increases in these ring frequencies upon electronic excitation signify that the nominal $n \rightarrow \pi^*$ chromophore is delocalized to include the conjugated ring atoms. The extent of this delocalization is different in the $T_1(n,\pi^*)$ vs $S_1(n,\pi^*)$ excited states. This conclusion is based on observed differences in T_1 vs S_1 ring fundamental frequencies.

Introduction

Molecular triplet states mediate a variety of photochemical processes.[1] Triplet intermediates are prominent in solution-phase photochemistry because of the ease of populating triplet states via $S_1 \rightsquigarrow T_1$ intersystem crossing, combined with the relatively long radiative lifetimes of the triplet species and their chemically reactive diradical electronic structures.

Spectroscopic characterization of triplet species can offer insights about these photochemical processes. Laser absorption or excitation spectra of gas-phase samples provide electronic excitation energies as well as vibrational frequencies. The triplet-state vibrational level patterns, along with Franck−Condon intensities, reveal changes in structure and dynamics accompanying excitation from the ground state. Recent work in our laboratory[2−5] has focused on the spectroscopy of small (monocyclic) organic molecules in $^3(n,\pi^*)$ excited states.

We have chosen molecules for these experimental studies so as to benefit the growing community of researchers[6] who investigate photochemical processes *computationally*. For a photochemical simulation to be successful, an accurate calculation of the relevant excited-state potential-energy surfaces is necessary, at least in regions pertinent to the transformation being studied. To verify or refine the excited-state potential calculations, experimental information about the excited states of model systems is required.

Our spectroscopic investigations[2−5] have provided such benchmark data on the lowest-energy $^3(n,\pi^*)$ states of conjugated enone molecules, including the prototype acrolein (CH_2═CH−CH═O)[4] as well as the simple cyclic enone 2-cyclopenten-1-one (2CP).[2,3] The latter is shown in Figure 1. Recent computational studies have used the spectroscopic information to test calculated triplet-state properties of these molecules.[7−10] These properties include adiabatic excitation energies as well as triplet-state vibrational frequencies.

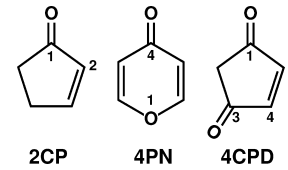

Figure 1. 2-Cyclopenten-1-one (2CP), 4*H*-pyran-4-one (4PN), and 4-cyclopentene-1,3-dione (4CPD).

Triplet excited states have received relatively little attention in spectroscopic studies, mainly because singlet → triplet transitions originating in the ground electronic state are nominally spin-forbidden. We have implemented the highly sensitive cavity ringdown (CRD)[11] and phosphorescence excitation (PE)[12] techniques to contend with the low oscillator strength of $T_1(n,\pi^*) \leftarrow S_0$ transitions.

Recently, we reported the $T_1(n,\pi^*) \leftarrow S_0$ PE spectrum of 4*H*-pyran-4-one (4PN),[5] a cyclic enone molecule that has more extensive conjugation into the ring than 2CP (see Figure 1). For both 2CP and 4PN, we observed effects of triplet $n \rightarrow \pi^*$ excitation on the ring vibrational modes. We found in each case that the energy-level structure for out-of-plane ring bending (the lowest-frequency mode) changes significantly upon triplet excitation. The observed changes indicate a decreased preference for planarity in the triplet state. This tendency also exists for the $S_1(n,\pi^*)$ excited states of both molecules but is much less pronounced in those cases.[13,14] For both 2CP and 4PN, we have concluded that the *triplet* $T_1(n,\pi^*) \leftarrow S_0$ chromophore is more delocalized to include the ring atoms than in the case of the analogous $S_1(n,\pi^*) \leftarrow S_0$ *singlet* excitation.

In this paper, we present and analyze the $T_1(n,\pi^*) \leftarrow S_0$ CRD absorption spectrum of 4-cyclopentene-1,3-dione (4CPD). The 4CPD molecule, shown in Figure 1, is a constitutional isomer of 4PN; both have a six-atom conjugated π system. In 4CPD, the conjugation resembles that of hexatriene, whereas the 4PN

† Part of the "Robert W. Field Festschrift".

* To whom correspondence should be addressed. E-mail: druckers@uwec.edu.

10.1021/jp9041364 CCC: $40.75
Published on Web 09/08/2009

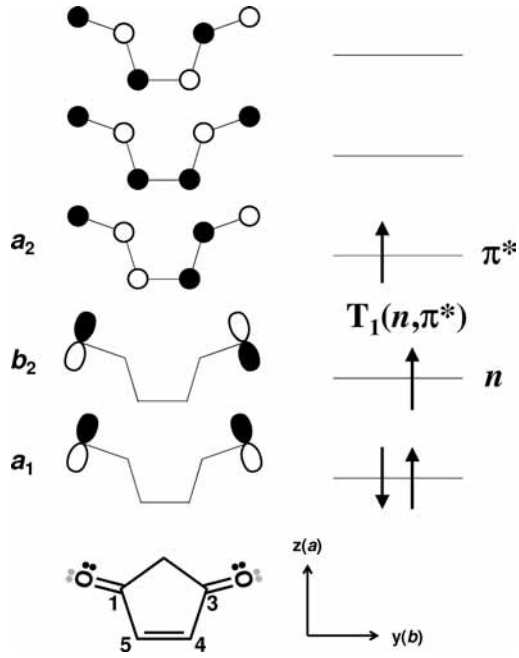

Figure 2. Schematic of the molecular orbitals in 4CPD, along with the coordinate system used in analyzing the $T_1(n,\pi^*) \leftarrow S_0$ spectrum. The same molecular orbital diagram applies to the $S_1(n,\pi^*)$ state, except the spin of the π^* electron is flipped (after ref 16).

molecule has a conjugated structure that is closer to benzenoid. Figure 2 shows schematically the highest occupied molecular orbitals of 4CPD. The two carbonyl groups give rise to two nonbonding orbitals of different symmetry in the C_{2v} molecular point group. The lowest-energy electronic transition involves promotion of an electron from the b_2 nonbonding orbital[15] to an a_2 π^* antibonding orbital. Hence, the electronic symmetry of the (n,π^*) upper state of the transition is $b_2 \times a_2 = B_1$. The electron occupancy shown in Figure 2 applies to both $T_1(n,\pi^*)$ and $S_1(n,\pi^*)$ excited states.

In 2000, Back and Gordon[16] reported the vibronically resolved $S_1(n,\pi^*) \leftarrow S_0$ ($B_1 \leftarrow A_1$) absorption spectrum of 4CPD in the gas phase. Their assignment and analysis of the spectrum were aided by a prior infrared and Raman study of the ground electronic state by Fortunato and Giorgini.[17] From the $S_1 \leftarrow S_0$ absorption spectrum, Back and Gordon determined fundamental frequencies in the S_1 excited state for 11 of the 27 vibrational modes of the molecule. The hot-band ($v'' > 0$) structure in the spectrum afforded several ground-state fundamentals in the gas-phase sample that had previously been determined[17] for the liquid only.

Back and Gordon found that the $S_1 \leftarrow S_0$ excitation in 4CPD causes the lowest ring-bending and -twisting frequencies to *increase*, rather than decrease as in 4PN and 2CP. The increases in 4CPD are attributable to the occupied π^* orbital in the excited state, which has bonding character within the ring at the C3−C4 and C1−C5 locations. The singlet $n \rightarrow \pi^*$ excitation strengthens these bonds and increases resistance to the bending and twisting motions of the ring.[16]

We undertook the present $T_1(n,\pi^*) \leftarrow S_0$ study of 4CPD to complement the work of Back and Gordon on the $S_1(n,\pi^*)$ state and, particularly, to continue exploring differences between triplet and singlet (n,π^*) excited states of the enones. As noted above, we found for the 2CP and 4PN molecules that the $T_1(n,\pi^*)$ and $S_1(n,\pi^*)$ states can differ substantially with respect to ring vibrational frequencies. Our objective in the present study of 4CPD was to investigate whether such differences are a general property of the cyclic enones. We were also interested in contributing further to the database of spectroscopic information for triplet excited states. The 4CPD molecule was a logical next choice for our investigations, being a structural isomer of 4PN and having the same ring size as 2CP.

We expect this series of molecules to offer a useful set of benchmark data for testing computed properties of excited states. The differences in $T_1(n,\pi^*)$ vs $S_1(n,\pi^*)$ vibrational frequencies, observed previously for 2CP[2] and 4PN[5]—and reported here for 4CPD—should be reproducible computationally by using high-level techniques. These frequency differences demonstrate the significance of configuration mixing, in which the triplet and singlet (n,π^*) states interact separately, in different manifolds, with higher excited states. The experimental results on the triplet states can potentially help computational chemists refine the treatment of configuration interaction, a central facet of any excited-state calculation.[18]

In this effort to use spectroscopy for advancing the progress of excited-state computations, we have taken advantage of current *computational* methods to guide our *spectroscopic* assignments. Below, we present vibrational frequency calculations for the S_0 ground state of 4CPD. These calculations use accurate[18] wave-function-based (CCSD) or density functional theory (B3LYP) approaches along with efficient code[19] and have allowed us to clarify several previously reported assignments[17] in the infrared spectrum. This clarification has aided the analysis of the hot-band structure we observe in the present $T_1 \leftarrow S_0$ CRD spectrum. We have also computed the $T_1(n,\pi^*)$ potential-energy minimum using the CIS(D) technique, the reliability of which has been well benchmarked.[7] This calculation has helped us establish the $T_1 \leftarrow S_0$ 0_0^0 band assignment in the CRD spectrum.

Experimental and Computational Details

The CRD spectroscopy system has been described previously in detail.[2] Briefly, the output of a Nd:YAG-pumped pulsed dye laser (Coumarin 460 or Coumarin 480 dye, approximately 0.5 mJ/pulse output at 480 nm) was sent through a spatial filter and then into a 1 m CRD cell. The cell was bounded by high-reflectivity mirrors (Los Gatos Research, quoted $R = 0.999\,95$ at 460 or 480 nm) with 6 m radii of curvature. The light exiting the cell was directed through a fiber-optic cable and detected by a photomultiplier (Electron Tubes P30A-08). The photomultiplier signal was sent into the 50 Ω input of a digital oscilloscope (10-bit vertical resolution) and through a 20 MHz internal low-pass filter. The decay traces from typically 16 laser pulses were averaged and then sent to a computer, where a monoexponential rate constant k_{obs} (along with baseline offset) was determined.

4-Cyclopentene-1,3-dione (95%) was purchased from Aldrich. The solid sample of 4CPD was subjected to several freeze−pump−thaw cycles, and its vapor was admitted to the previously evacuated CRD cell at room temperature. The vapor pressure, as measured by a capacitance manometer, was approximately 0.5 Torr (65 Pa). The stainless-steel cell was exposed repeatedly to the vapor in order to passivate the cell wall before spectroscopic measurements were made.

CRD spectra were recorded by plotting $k_{obs} - k_{empty}$ (where k_{empty} is the CRD decay constant of the evacuated cell) vs vacuum-corrected wavelength. The laser was advanced in increments of 0.005 nm within a scan. The resulting CRD spectra contained a sinusoidal noise component attributable to an etalon effect between the parallel surfaces of each mirror.

In some cases, the noise was smoothed by averaging each point in the spectrum with the five preceding and following points. This procedure had a minimal effect on the peak heights or bandwidths of the spectral features.

Computations were carried out using the Q-Chem 3.2 quantum-chemistry package.[19] The geometry of 4CPD in its S_0 electronic state was fully optimized using coupled-cluster theory at the single and double substitution operator (CCSD)[20] level. Vibrational frequencies in the S_0 state were determined in the harmonic approximation using analytical second derivatives. The ground-state calculations were also done using density functional theory (DFT) with Becke (1988)[21] exchange and Lee−Yang−Parr[22] correlation functionals (B3LYP). The 6-311+G(d,p) basis set was used for all of the ground-state calculations described above.

The 0−0 excitation energy for the $T_1(n,\pi^*) \leftarrow S_0$ transition was also calculated. The approach of Grimme and Izgorodina[7] was used, which employs DFT as an efficient means for geometry optimization, followed by accurate, more computationally intensive methods for calculating absolute energy at the DFT-optimized geometry. In the present application, the S_0 ground-state geometry of 4CPD was optimized using the B3LYP method. The resulting geometry was used as input for a single-point energy calculation employing Møller−Plesset perturbation theory of order 2 (MP2). The process was repeated for the $T_1(n,\pi^*)$ state, using time-dependent density functional theory (TDDFT-B3LYP) to determine an optimized excited-state geometry. The excited-state energy at this geometry was calculated by applying the resolution of the identity technique to configuration interaction singles with a correction for double excitation (RI-CIS(D)). Zero-point corrections to the MP2 and RI-CIS(D) energies were made using vibrational frequencies calculated by DFT-B3LYP for the ground state (as described in the previous paragraph) and TDDFT-B3LYP for the excited state. The 0−0 excitation energy for the $T_1 \leftarrow S_0$ transition was taken as the difference between the zero-point-corrected RI-CIS(D) and MP2 energies. The cc-pVTZ basis set[23] was used for all calculations (except the DFT-computed ground-state frequencies) leading up to the 0−0 excitation energy.

The foregoing procedure was also used to determine the 0−0 excitation energy for the $S_1(n,\pi^*) \leftarrow S_0$ transition of 4CPD. Because this value is known from previous experimental work,[16] the $S_1 \leftarrow S_0$ calculation serves as one benchmark (among others)[7] for testing the accuracy of the computational technique we have applied to the $T_1 \leftarrow S_0$ transition.

Results and Discussion

Computational Results. The $S_1 \leftarrow S_0$ spectrum of 4CPD reported by Back and Gordon[16] contains a rich structure of vibronic hot bands, and the analysis and interpretation of that spectrum[16] relied heavily on knowledge of the vibrational level structure and mode descriptions in the S_0 ground electronic state. We expected that the analysis of the present $T_1 \leftarrow S_0$ spectrum would proceed similarly. We undertook the computational study of the ground-state vibrational frequencies in order to verify previous assignments[17] of the infrared and Raman spectra. Assignments in the gas-phase infrared spectrum previously afforded fundamentals for most of the a_1 vibrational modes; the remaining fundamentals were determined from the Raman or infrared spectra of 4CPD in the solid or liquid phase.[17] Furthermore, the hot-band structure in the $S_1 \leftarrow S_0$ spectrum suggested gas-phase values for the lowest-frequency (<400 cm^{-1}) fundamentals, including those of a_1, a_2, and b_1 symmetry.[16]

TABLE 1: Computed and Experimental Fundamental Frequencies (cm^{-1}) for the S_0 State of 4CPD

sym[a]	mode no.	CCSD	B3LYP	obs[b]	meas type
a_1	1	3260	3221		
	2	3107	3065	3073	liquid Raman
	3	1863	1813	1857[c]	solid IR
	4	1648	1620	1635[c]	solid IR
	5	1448	1418	1392	gas IR
	6	1283	1239	1242	gas IR
	7	1086	1074	1057	gas IR
	8	861	843	842	liquid Raman
	9	580	577	588	gas IR
	10	393	388	385[d]	gas $S_1 \leftarrow S_0$ hot band
a_2	11	1159	1129	1125	solid IR
	12	983	1011	1014[e]	liquid
	13	635	646	637[d]	gas $S_1 \leftarrow S_0$ hot band
	14	236	241	239[d]	gas $S_1 \leftarrow S_0$ hot band
b_1	15	3159	3105		
	16	970	964	951[f]	liquid
	17	797	803	784	gas IR
	18	437	440	424[g]	liquid
	19	75	93	99[d]	gas $S_1 \leftarrow S_0$ hot band
b_2	20	3238	3201		
	21	1828	1778	1786[c]	solid IR
	22	1366	1341	1322	gas IR
	23	1275	1234	1227	liquid IR
	24	1169	1141	1130	liquid IR
	25	842	813	808	gas IR
	26	699	693	699[c]	liquid IR
	27	529	527	522	gas IR

[a] The coordinate system in Figure 1 is the same as that used by Back and Gordon (ref 16), but our choice of x and y axes is reversed from that of Fortunato and Giorgini (ref 17); consequently, the b_1 and b_2 labels here are reversed from those of ref 17, and the mode numbering is different for ν_{15} and higher. [b] Reference 17 except where noted. [c] Reassignment based on frequencies computed here. [d] Reference 16. [e] Inferred from 1537 cm^{-1} − 523 cm^{-1} Raman combination difference. [f] Inferred from 1200 cm^{-1} − 249 cm^{-1} Raman combination difference. [g] Inferred from 673 cm^{-1} (IR) − 249 cm^{-1} (Raman) combination difference.

The computations presented here have confirmed many of the S_0 vibrational assignments and suggested corrections for several others; as a result, we have been able to rely quantitatively on frequencies from the gas-phase spectra. This has benefited our vibronic analysis of the $T_1 \leftarrow S_0$ spectrum, as we describe later.

Table 1 shows the ground-state fundamentals computed by both CCSD and B3LYP techniques. No scale factors were applied. Also included in Table 1 are frequencies from the previous spectroscopic studies.[16,17] For each of the vibrational modes below 700 cm^{-1}, the average of the CCSD and B3LYP calculated frequencies is within 15 cm^{-1} (typically 2% or less) of the observed. At higher frequencies, calculated values are all within 5% of observed.

The entries in Table 1 imply reassignments for several features[17] in the vibrational spectra. The reassignments improve the agreement between observed and computed fundamental frequencies. For the purpose of analyzing the present $T_1 \leftarrow S_0$ electronic spectrum, the most important reassignment involves a band observed at 673 cm^{-1} in the liquid-phase infrared spectrum. This band was originally assigned[17] to ν_{26} (b_2 in-plane carbonyl bend). We suggest that this feature is instead the $\nu_{14} + \nu_{18}$ ($a_2 \times b_1 = b_2$) combination band. This reassignment implies that the ν_{18} (b_1 out-of-plane carbonyl wag) fundamental frequency is approximately $673-249 = 424$ cm^{-1} (in the liquid), which differs by 3% from its computed (gas-

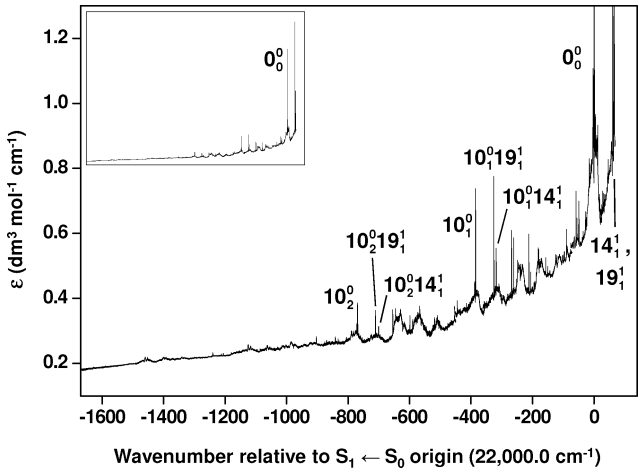

Figure 3. Survey CRD scan of 4CPD in the $S_1 \leftarrow S_0$ hot-band region. The inset is scaled to show the intensity of the $S_1 \leftarrow S_0$ origin relative to the hot bands.

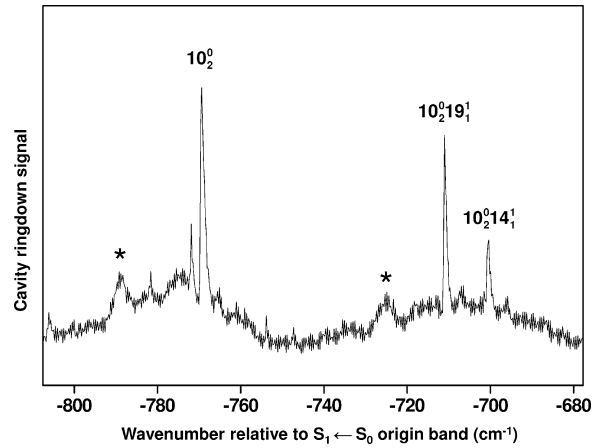

Figure 4. Expanded view of the spectrum in Figure 3. Bands marked with asterisks are assigned to the 10_0^2 and $10_0^2 19_1^1$ transitions of the $T_1 \leftarrow S_0$ system.

phase) value. We believe the reassignment is warranted because ν_{18} had been previously assigned to the infrared band at 699 cm^{-1}, which is 38% larger than the value we have computed for ν_{18} (mean of CCSD and B3LYP). Such a discrepancy would be wildly inconsistent with errors for the other fundamentals. The band at 699 cm^{-1} is now assigned as the ν_{26} fundamental (b_2 in-plane carbonyl bend). This differs from the mean computed ν_{26} frequency by only 0.4%.

A separate computational focus in this work was the 0−0 excitation energy for the $T_1(n,\pi^*) \leftarrow S_0$ transition of 4CPD. Using the approach of Grimme and Izgorodina,[7] we calculated the 0−0 excitation energy to be 2.63 eV. (The adiabatic excitation energy, i.e., without zero-point correction, was determined to be 2.67 eV.) As we discuss below, the 0−0 calculation supports a $T_1 \leftarrow S_0$ origin-band assignment for the feature observed at 20 540 cm^{-1}, or 2.55 eV, in the CRD spectrum.

As a computational benchmark, we also calculated the 0−0 excitation energy for the $S_1(n,\pi^*) \leftarrow S_0$ transition. The computed value is 2.82 eV, compared to 2.73 eV established by the experimental work of Back and Gordon.[16]

Vibronic Analysis. Figure 3 is a CRD survey spectrum of 4CPD. The $S_1(n,\pi^*) \leftarrow S_0$ origin band (22 000.0 cm^{-1}) is at the high-wavenumber end of the region shown, and the observed vibronic structure at lower wavenumber is due to hot bands associated with the $S_1 \leftarrow S_0$ system.[16] Examination of these hot bands will help in the discussion and analysis of the $T_1 \leftarrow S_0$ band system, detected 1460 cm^{-1} below the $S_1 \leftarrow S_0$ origin. The spectrum in Figure 3 is highly structured and contains a progression of $S_1 \leftarrow S_0$ hot bands ($v'' = 1$ and $v'' = 2$) assigned previously[16] to the totally symmetric ring mode ν_{10}. This mode is the lowest-energy vibration of a_1 symmetry, with a fundamental frequency of 385 cm^{-1} in the ground electronic state.[16,17] Attached to each member of the hot-band progression, as well as the $S_1 \leftarrow S_0$ origin, are $\Delta v = 0$ sequence bands assigned[16] to the out-of-plane ring-bending and -twisting modes, ν_{19} (b_1) and ν_{14} (a_2), respectively. These are the two lowest-energy vibrations in the molecule, with fundamental frequencies of 99 and 239 cm^{-1}, respectively, in the ground electronic state.[16,17]

Figure 4 shows an expanded view of the $S_1 \leftarrow S_0$ hot-band region near −750 cm^{-1} relative to the origin. The region in Figure 4 contains the 10_2^0 overtone transition at −770 cm^{-1}, as well as 19_1^1 and 14_1^1 sequences attached to the 10_2^0 band. Each of these bands has a relatively sharp room-temperature rotational contour that is typical of a dipole-allowed *c*-type (*x*-polarized) transition within the $S_1 \leftarrow S_0$ ($B_1 \leftarrow A_1$) band system.[16] However, two less intense features appear in the vicinity that are significantly broader. These bands (marked with asterisks in Figure 4) are not assigned to the $S_1 \leftarrow S_0$ system because their rotational contours do not match those of the allowed *c*-type transitions nor those of the diffuse, vibronically induced *a*- or *b*-type. (An example of the latter is seen near −600 cm^{-1} in Figure 3.)

The weaker, broader bands in Figure 4 were not reported by Back and Gordon, nor were others, with similar contours, that extend several hundred cm^{-1} further to the red. The contrasting contours in Figure 4 suggest that the unassigned bands are part of a singlet−triplet absorption system, i.e., $T_1(n,\pi^*) \leftarrow S_0$. The rotational selection rules for such transitions are much different from the $S_1(n,\pi^*) \leftarrow S_0$ selection rules; the shape of the $T_1(n,\pi^*) \leftarrow S_0$ band contour depends upon the singlet states (most likely nearby $^1(\pi,\pi^*)$ states) coupled to T_1 by spin−orbit interaction and from which the $T_1 \leftarrow S_0$ transition obtains its oscillator strength.[24] The bands within the $T_1 \leftarrow S_0$ system also contain *O*- and *S*-form branches in addition to the *P*-, *Q*-, and *R*-forms.[24]

Figure 5 shows a vertically expanded spectral region beginning about 700 cm^{-1} lower than in Figure 4, or 1500 cm^{-1} below the $S_1 \leftarrow S_0$ origin. The $T_1 \leftarrow S_0$ origin band is assigned to the feature whose maximum intensity is at 20 540.0 ± 0.5 cm^{-1} (486.849 nm). This assignment is based on the following considerations:

(1) The band at 20 540.0 cm^{-1} marks an abrupt onset of detectable transitions. The intensities grow as the wavenumber increases. This observation is consistent with an origin-band assignment for the 20 540.0 cm^{-1} feature, because any transition to lower wavenumber would correspond to a hot band and would have a diminished intensity. At higher wavenumber, one expects progressions of Franck−Condon-allowed transitions with growing intensity envelopes.

(2) Under the proposed assignment for the $T_1 \leftarrow S_0$ origin, the ratio of the $T_1 \leftarrow S_0$ to $S_1 \leftarrow S_0$ origin-band intensities is approximately 0.005. (The observed molar absorptivity (ε) values are approximately 0.01 and 2.0 $dm^3\ mol^{-1}\ cm^{-1}$, respectively.) An intensity ratio of this magnitude is common for spin-forbidden vs allowed $n \rightarrow \pi^*$ transitions.[25]

(3) The assigned $T_1 \leftarrow S_0$ origin band is 1460.0 cm^{-1} below the $S_1 \leftarrow S_0$ origin. A singlet−triplet separation of this magnitude is similar to the splittings found in structurally related cyclic enones, such as 2CP,[2] 4PN,[5] and 2-cyclohexen-1-one.[4]

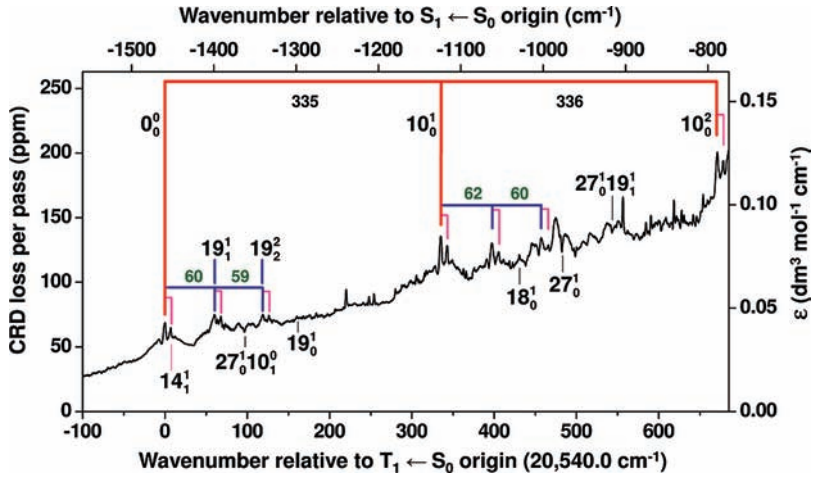

Figure 5. CRD spectrum of 4CPD, indicating assignments in the $T_1 \leftarrow S_0$ band system. Numerical values in between tie lines indicate wavenumber (cm^{-1}) separations between sequence or progression members. A sinusoidal noise component in the original spectrum was smoothed according to a procedure described in the text.

In these molecules, the lowest (n,π^*) triplet state is lower than the isoconfigurational singlet excited state by 1260, 1069, and 1520 cm^{-1}, respectively.

(4) The $T_1 \leftarrow S_0$ excitation energy obtained from the assigned origin-band position is very close to the calculated 0−0 excitation energy we report above. The calculated value is 0.08 eV greater than the observed. The well-benchmarked computational approach is that of Grimme and Izgorodina,[7] who calculated $n \rightarrow \pi^*$ 0−0 excitation energies in a series of seven other compounds, including prototypical enones acrolein and 2CP. The calculated 0−0 energies (including singlet−singlet and singlet−triplet excitations) are typically higher than observed, with a mean signed deviation (calculated − observed) of +0.09 eV. The present work adds another benchmark calculation, namely, the 0−0 excitation energy for the S_1(n,π^*) $\leftarrow S_0$ transition of 4CPD. This computed value is 0.09 eV greater than observed. Thus, the deviation we observe for the calculated $T_1 \leftarrow S_0$ excitation energy, +0.08 eV, is consistent in both magnitude and direction with all of the existing benchmark calculations using the technique of Grimme and Izgorodina. This result fully supports our spectral assignment of the $T_1 \leftarrow S_0$ origin band.

(5) Attached to the 20 540.0-cm^{-1} band, and extending to higher wavenumber, is a series of at least three detectable bands at intervals of 335−336 cm^{-1}. These intervals compare to the spacings of 336−337 cm^{-1} between members of the ν'_{10} progression in the $S_1 \leftarrow S_0$ band system.[16] The similarity suggests an analogous ν'_{10} progression for the $T_1 \leftarrow S_0$ band system. Moreover, at 386 cm^{-1} below 20 540.0 cm^{-1}, we observe an exceedingly weak feature (Figure 6), just at the detection threshold of our CRD spectrometer. This interval matches the ν''_{10} fundamental frequency in the ground electronic state.[16,17] Thus, the 20 540.0-cm^{-1} band very likely marks a division between a ν'_{10} progression to the blue and a ν''_{10} progression to the red, consistent with a $T_1 \leftarrow S_0$ origin assignment for this band.

Figure 5 and Table 2 indicate additional vibronic band assignments for the $T_1 \leftarrow S_0$ system.

Attached to the 0_0^0 band, as well as each member of the ν'_{10} progression, is a band of slightly lower intensity appearing about 60 cm^{-1} higher in wavenumber. These bands can be assigned as combinations with the 19_1^1 sequence transition. This assignment is based on the very close similarity between the 19_1^1 sequence intervals in the $S_1 \leftarrow S_0$ band system[16] and those

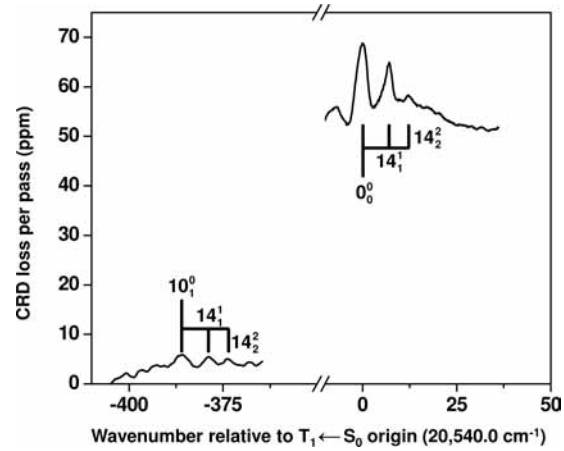

Figure 6. CRD spectrum of 4CPD in the low-wavenumber region of the $T_1 \leftarrow S_0$ band system. The CRD signal (photon loss) is greater in the origin region than the 10_1^0 hot-band region because the origin band sits on a broad baseline consisting of many unresolved sequence bands of the type N_1^1.

proposed for the $T_1 \leftarrow S_0$ system. In both band systems, the 19_1^1 transition is observed near 60 cm^{-1} relative to the 0_0^0 band, and in both systems, this interval increases about 1.5 cm^{-1} for each increasing value of v in the 10_0^v progression.

Further support for the 19_1^1 sequence assignment comes from observation of a very weak band at 160.5 cm^{-1} relative to the origin. This band is assigned to the 19_0^1 transition, which is predicted at (99 + 60.2 = 159) cm^{-1}, based on the 19_1^1 assignment at +60.2 cm^{-1}, and the ground-state combination difference of 99 cm^{-1} established in the previous $S_1 \leftarrow S_0$ work.[16] The 19_0^1 band is weak because ν_{19} is an antisymmetric (out-of-plane, b_1) mode, and hence, its Δv = odd electronic transitions have vanishing Franck−Condon factors. The very good agreement between the observed and anticipated 19_0^1 band position supports the 19_1^1 assignment in the present $T_1 \leftarrow S_0$ spectrum.

We also clearly detect bands in this spectrum that are assignable as 19_2^2 sequences. The ν_{19} mode has has the lowest ground-state frequency (99 cm^{-1}) in the molecule. Hence, the Boltzmann population of the ground-state $v''_{19} = 2$ level is appreciable, so the 19_2^2 sequence and its combinations with 10_0^v transitions are readily observed. For ν_{19}, the Boltzmann population ratio of the v'' to $v'' + 1$ levels is 0.6, which is similar to

TABLE 2: Vibronic Band Assignments (cm^{-1}) in the CRD Spectrum of 4CPD (* Denotes Vibronically Induced Band)

band position[a]	$T_1 \leftarrow S_0$ assignment	$S_1 \leftarrow S_0$ assignment
−386.4	10_1^0	
−379.2	$10_1^0 14_1^1$	
−374.3	$10_1^0 14_2^2$	
−168.2	?[c]	
−128.2	?[c]	
−48.7	10_1^1	
−6.8	18_1^1	
0	0_0^0	
7.1	14_1^1	
12.2	14_2^2	
60.2	19_1^1	
68.1	$14_1^1 19_1^1$	
96.7	$10_1^0 27_0^1$	
119.0	19_2^2	
126.3	$14_1^1 19_2^2$	
160.5	19_0^1*	
220.0		6_1^0 [−1240.0][b]
247.9		? [−1212.1][d]
254.0		? [−1206.0][d]
279.9		$6_1^0 19_1^1$ [−1180.1]
305.2		10_3^0 [−1154.8]
328.4	$10_0^1 18_1^1$	
335.2	10_0^1	
342.8	$10_0^1 14_1^1$	
348.9	$10_0^1 14_2^2$	
362.3		$10_3^0 19_1^1$ [−1097.7]
365.9		$10_3^0 14_1^1 19_1^1$ [−1094.1]
397.3	$10_0^1 19_1^1$	
405.6	$10_0^1 14_1^1 19_1^1$	
411.1	$10_0^1 14_2^2 19_1^1$	
430.3	18_0^1*	
454.3		$10_2^0 14_1^0$ [−1005.7]*
457.1	$10_0^1 19_2^2$	
465.7	$10_0^1 14_1^1 19_2^2$	
482.2	27_0^1*	
512.9		$10_2^0 14_1^0 19_1^1$ [−947.1]*
542.9	$19_1^1 27_0^1$*	
556.1		$6_1^0 10_0^1$ [−903.9]
618.3		$6_1^0 10_0^1 19_1^1$ [−841.7]
627.7		$6_1^0 10_0^1 14_1^1$ [−832.3]
671.3	10_0^2	
678.3	$10_0^2 14_1^1$	
734.7	$10_0^2 19_1^1$	
796.0	$10_0^2 19_2^2$	
800.1	$10_0^2 14_1^1 19_2^2$	
837.6		$10_1^0 14_1^0$ [−622.4]*
897.2		$10_1^0 14_1^0 19_1^1$ [−562.8]*
1006.4	10_0^3	
1072.0	10019_1^1	
1138.0	$10_0^3 19_2^2$	

[a] Relative to the $T_1 \leftarrow S_0$ origin band observed at 20 540.0 ± 0.5 cm^{-1}. [b] The bracketed value indicates the band position relative to the $S_1 \leftarrow S_0$ origin band at 22 000.0 cm^{-1} (ref 16). [c] Unassigned band with broad contour similar to those assigned to the $T_1 \leftarrow S_0$ system. [d] Unassigned band with narrow contour similar to those assigned to the $S_1 \leftarrow S_0$ system.

the intensity ratios observed for the 0_0^0, 19_1^1, and 19_2^2 bands assigned in the $T_1 \leftarrow S_0$ spectrum.

Attached to the 0_0^0 and 10_1^0 bands, as well as each member of the 10_0^v progression and its $10_0^v\ 19_1^1$ and $10_0^v\ 19_2^2$ combinations, is a satellite band appearing about 7 cm^{-1} higher in wavenumber. We assign these bands as combinations with the 14_1^1 sequence transition. This sequence interval is very *different* from that observed for ν_{14} in the $S_1 \leftarrow S_0$ band system. In the singlet case, the 14_1^1 sequences are observed about 65 cm^{-1} higher than their parent bands, whereas these intervals are only 7 cm^{-1} higher in the triplet band system, according to our assignments.

Despite this significant difference, a 14_1^1 assignment is reasonable for the +7 cm^{-1} satellite bands observed in the $T_1 \leftarrow S_0$ system. This is because the ν_{14} mode has the second lowest fundamental frequency (239 cm^{-1}) in the ground state, and hence, its $v'' = 1$ level is sufficiently well populated at room temperature to afford the relatively high intensities observed for the +7 cm^{-1} satellites. Also, assuming these satellites must correspond to N_1^1 sequence transitions, no mode of higher frequency than ν_{14} is a reasonable candidate for N. The next higher-frequency mode in this molecule is ν_{10} (385 cm^{-1} in the ground state); however, the 10_1^1 sequence band is predicted at 335−385 = −50 cm^{-1} relative to the 0_0^0 band, according to the ν'_{10} assignments discussed above. A weak transition, assigned to 10_1^1, is observed at −48.7 cm^{-1}. After ν_{10}, the next higher-frequency mode is ν_{18} (b_1, out-of-plane carbonyl wag), with a ground-state fundamental of approximately 424 cm^{-1} (based on our reassignment, described above, of the liquid-phase infrared spectrum). For ν_{18}, the $v'' = 1$ Boltzmann population factor is 0.13, which is inconsistent with the observed intensities of the +7 cm^{-1} satellites. Thus, we maintain a 14_1^1 assignment for these bands.

To summarize the essential parts of the vibronic analysis, most of the $T_1 \leftarrow S_0$ bands in the 700 cm^{-1} region above the origin are assignable either to members of the ν'_{10} progression or to combinations of 10_0^v transitions with ν_{19} or ν_{14} sequences. All of these transitions have nonvanishing Franck−Condon factors, stemming from the a_1 symmetry of ν_{10} and the $\Delta v = 0$ assignments on the ν_{19} and ν_{14} (b_1 and a_2, respectively) sequences.

(At wavenumbers greater than 200 cm^{-1}, the spectrum becomes increasingly overlapped with hot bands belonging to the $S_1 \leftarrow S_0$ system. Their onset is about 1200 cm^{-1} below the $S_1 \leftarrow S_0$ origin. These hot bands have distinctive contours,[26] and it is straightforward to identify them as part of the $S_1 \leftarrow S_0$ system. Table 2 includes these bands and extends the $S_1 \leftarrow S_0$ assignments of Back and Gordon.)

The $T_1 \leftarrow S_0$ bands summarized above and shown in Figures 5 and 6 have rotational contours that are similar to each other and significantly broader than most of the $S_1 \leftarrow S_0$ contours. Several other $T_1 \leftarrow S_0$ bands are broader still. One of these is the 19_0^1 transition observed at 160.5 cm^{-1}. As mentioned above, this band is weak because the $\Delta v = 1$ transition involving a b_1 vibrational mode is Franck−Condon-forbidden. The 19_0^1 transition presumably derives its intensity from vibronic interaction within the triplet manifold. Vibronic coupling has been invoked previously to explain symmetry-forbidden transitions observed in the $T_1 \leftarrow S_0$ spectra of 2CP,[2] 4PN,[5] and pyrazine.[12]

Another weak feature with a similarly broad contour is observed at 430.3 cm^{-1}. This band is tentatively assigned to the next higher-frequency mode of b_1 symmetry, ν_{18} (out-of-plane carbonyl wag). An alternative candidate is ν_{27} (b_2 in-plane ring distortion, 522 cm^{-1} in the ground state), but we prefer the 18_0^1 assignment for the band at 430.3 cm^{-1} because it correctly predicts the 18_1^1 sequence-band position. The ν''_{18} fundamental in the ground state can be taken from the calculation presented earlier (439 cm^{-1}, the mean of the CCSD and B3LYP values) or from the liquid-phase infrared spectrum (424 cm^{-1}, based on our reassignment described above). These values, combined with the assigned 18_0^1 band position at 430.3 cm^{-1}, predict the 18_1^1 band at either 430.3 − 439 = −8.7 cm^{-1} or 430.3 − 424 = +6.3 cm^{-1}. Given the uncertainty in the computed low-frequency fundamentals (average unsigned error of 6.1 cm^{-1} for B3LYP and 9.1 cm^{-1} for CCSD), or spectral shifts up to 20 cm^{-1} between gas- and liquid-phase infrared

TABLE 3: Fundamental Vibrational Frequencies (cm^{-1}) in the S_0, T_1, and S_1 States of 4CPD

mode no.	S_0[a]	$T_1(n,\pi^*)$[b]	$S_1(n,\pi^*)$[c]	approx description
10 (a_1)	385.0	335.2	336.5	sym in-plane ring distortion
14 (a_2)	239	246	307	ring twist
18 (b_1)	424[d]	430.1		sym out-of-plane carbonyl wag
19 (b_1)	99	160.5	160	ring bend
27 (b_2)	522[e]	482.2		antisym in-plane ring distortion

[a] From the hot band in the gas-phase $S_1 \leftarrow S_0$ spectrum (ref 16) unless otherwise noted. [b] This work. [c] From the $S_1 \leftarrow S_0$ spectrum (ref 16). [d] Liquid-phase value inferred from ref 17 (seeTable 1). The gas-phase value computed in the present work (mean of CCSD and B3LYP) is 439 cm^{-1}. [e] From the gas-phase IR spectrum (ref 17).

TABLE 4: Lowest-Energy Ring Frequencies (cm^{-1}) in the S_0, T_1, and S_1 States of Cyclic Conjugated Enones

molecule and mode	S_0[a]	$T_1(n,\pi^*)$[b]	$S_1(n,\pi^*)$[c]
2CP twist	287	239	274
2CP bend	94	37	67
4PN twist	395	269	260
4PN bend	149	126	145
4CPD twist	239	246	307
4CPD bend	99	161	160

[a] 2CP, ref 29; 4PN, ref 30; 4CPD, ref 16. [b] 2CP, ref 2; 4PN, ref 5; 4CPD, this work. [c] 2CP, ref 13; 4PN, ref 14; 4CPD, ref 16.

features, the 18_1^1 prediction agrees well with a band observed at -6.8 cm^{-1} in the present CRD spectrum. This band is Franck−Condon-allowed but weak because of a low (0.13) Boltzmann factor.

Finally, we observe an intense feature consisting of two very broad peaks centered at 21 022.7 cm^{-1}, or + 482.2 cm^{-1} relative to the $T_1 \leftarrow S_0$ origin. The band profile is different from that of any of the $T_1 \leftarrow S_0$ bands we have discussed. It is unlikely that this broad feature belongs to the $S_1 \leftarrow S_0$ system, because it appears about 980 cm^{-1} below the $S_1 \leftarrow S_0$ origin. This corresponds to a Boltzmann factor of only about 0.01 if the band were assigned to an $S_1 \leftarrow S_0$ hot-band transition with no vibrational excitation in the upper state. Moreover, the symmetry-allowed $S_1 \leftarrow S_0$ bands have exceedingly narrow profiles (see Figure 3), so the very broad feature under discussion would have to be vibronically induced. We conclude that the low oscillator strength and Boltzmann factor for such an $S_1 \leftarrow S_0$ transition would make it undetectable in the present experiment.

We therefore maintain that the feature at +482.2 cm^{-1} relative to the $T_1 \leftarrow S_0$ origin does indeed belong to the triplet band system. Less intense bands having the same profile are observed about 60 and 120 cm^{-1} higher in wavenumber, and 385 cm^{-1} lower. These support a $T_1 \leftarrow S_0$ assignment for the main band and are identified as 19_1^1, 19_2^2, and 10_1^0 combinations, respectively, with the parent.

The parent band at 482.2 cm^{-1} is tentatively assigned[27] to the 27_0^1 transition. Mode 27, an in-plane ring distortion, is the lowest-frequency vibration of b_2 symmetry. It is the antisymmetric analog of the ν_{10} (a_1) mode. As indicated earlier in this section, the ν_{10} fundamental frequency drops by 50 cm^{-1}, or 13%, upon $T_1 \leftarrow S_0$ excitation. Under the 27_0^1 assignment for the 482.2 cm^{-1} band, the ν_{27} fundamental drops by 41 cm^{-1}, or 8%. These percentage reductions are roughly the same magnitude. The small difference in the percentages can be rationalized in terms of contributions made by internal coordinates to the two modes. A normal-mode analysis of 4CPD[17] shows that both ν_{10} and ν_{27} involve in-plane carbonyl bending and CH_2−CHO stretching, whereas only ν_{27} involves CH−CHO stretching. The latter (which pertains to the C1−C5 and C3−C4 bonds) is expected to become more stiff upon $n \rightarrow \pi^*$ excitation (see the Introduction) and would therefore offset the reduction of the ν_{27} frequency.

Effects of $n \rightarrow \pi^*$ Excitation. Table 3 lists the fundamental frequencies for the $T_1(n,\pi^*)$ excited state of 4CPD determined from the above vibronic analysis. For a given vibrational mode N, the frequency listed was derived either from the N_0^1 band in the CRD spectrum or from the N_1^1 sequence-band position in the CRD spectrum along with the known $v'' = 1-0$ ground-state combination difference, depending on which CRD band measurement was more precise. For comparison, the table also includes available $S_1(n,\pi^*)$ excited-state frequencies obtained from the $S_1 \leftarrow S_0$ spectrum of Back and Gordon[16] and S_0 ground-state frequencies from either the $S_1 \leftarrow S_0$ spectrum or the vibrational spectra of Fortunato and Giorgini.[17]

As seen in Table 3, the $n \rightarrow \pi^*$ transition causes the frequencies of out-of-plane ring vibrations (bend and twist) to increase for both singlet and triplet excitation. This indicates that the nominal carbonyl chromophore is delocalized to include the ring atoms in each case. However, the precise effects on the ring vibration differ for the two excited states. Whereas the S_1 and T_1 states show the same 60% increase in ring-*bending* frequency compared to the ground state, only the S_1 state has a substantially increased ring-*twisting* frequency: 28%, compared to 3% for T_1.

To gain insight on the differing S_1 and T_1 ring-twisting frequencies, it is helpful to consider again the lowest π^* orbital in the six-atom conjugated system (Figure 2). When an electron is promoted to this orbital, the ring vibrations increase in frequency because the C3−C4 and C1−C5 bond orders increase. At the same time, however, the C4═C5 bond order *decreases* because the π^* orbital has antibonding character between C4 and C5. This offsets the frequency increase for ring twisting,[16] a mode that substantially involves torsion about the C═C bond. The observed increase in ring-twisting frequency is smaller for T_1 than for S_1, suggesting that the weakening of the C═C bond is more extensive in the T_1 state. This weakening would not have a direct effect on ring *bending* because of the symmetry of that vibration, and is in accord with our observation that the ring-bending frequencies are the same in the two excited states.[28]

In summary, the $n \rightarrow \pi^*$ chromophore extends to the ring atoms for both the S_1 and T_1 excitation of 4CPD, but the ring C═C bond appears to be weakened more in the T_1 state. As mentioned in the Introduction, we have observed similar tendencies in structurally related enones. Table 4 shows changes in ring-bending and ring-twisting frequencies upon $n \rightarrow \pi^*$ excitation for the molecules 2CP, 4PN, and 4CPD (whose structures are all shown in Figure 1).

For 2CP, the ring-twisting and -bending fundamentals both drop more significantly for T_1 than for S_1 excitation. Furthermore, one-dimensional potential fits to the ring-bending vibronic data show that the T_1 state of 2CP has a bent equilibrium geometry,[2] with a small (43 cm^{-1}) barrier to planarity, whereas the S_1 geometry is planar[13] (as is the ground state).[29] In the case of T_1 excitation, the forces favoring ring planarity (i.e., associated with the conjugation) are weakened significantly and

are apparently outweighed by torsional forces that would push the atoms out of a coplanar arrangement.

In the 4PN molecule as well, the conjugation of the ring atoms is significantly disrupted upon $T_1(n,\pi^*)$ excitation. The ring-twisting fundamental frequency in the T_1 state (as well as $S_1(n,\pi^*)$) is about 30% lower than in the ground state.[30] The large drop is not surprising, because this mode significantly involves torsion about the two C=C double bonds in the ring. The $n \rightarrow \pi^*$ excitation reduces their bond orders and thereby diminishes resistance to the torsional motion.

Similar considerations pertain to the ring-bending mode of 4PN, although the effect appears to be limited to the T_1 state in this case. This vibration involves a wagging motion of the O-1 atom out of the molecular plane. This motion is resisted by virtue of the O-1 atom linking the two ends of the conjugated chain. The conjugation may also be viewed as extending to the O-1 atom in benzenoid fashion and stabilizing the coplanar geometry of all the ring atoms. The T_1 ring-bending frequency is 15% lower than in the ground state, suggesting that the O-1 atom becomes less involved in the conjugation. It is notable, though, that the S_1 ring-bending frequency is *barely reduced* from its ground-state value. These observations indicate that in 4PN, as in the case of 2CP, the conjugation is more disrupted for triplet than singlet excitation.

To summarize the results for the three conjugated enones, 2CP, 4PN, and 4CPD, the $n \rightarrow \pi^*$ chromophore is delocalized to include the ring atoms for both T_1 and S_1 excitation. Moreover, antibonding character within the ring appears to be greater for each of the T_1 states. This is manifested in different particular ways for each molecule. 2CP and 4CPD provide an interesting comparison because they have the same arrangement of heavy atoms in the ring. In 2CP, the T_1 state[2] has a nonplanar equilibrium geometry and a flatter ring-twisting potential than S_1[13] or S_0.[29] For 4CPD, with more extensive conjugation, we have shown here that the ring-twisting vibration *stiffens* upon $T_1 \leftarrow S_0$ excitation. The increase in fundamental frequency is less for T_1 than for S_1 excitation. We propose that the C=C moiety has enhanced antibonding character in the T_1 state, causing the ring-twisting potential to be less steep in T_1 than in S_1.

In future work, we would like to investigate the carbonyl part of the $n \rightarrow \pi^*$ chromophore in 4CPD. The observations presented above suggest that T_1 excitation involves more extensive ring delocalization than in S_1. This implies that the carbonyl bond, outside the ring, would be less affected by T_1 than S_1 excitation. In the present CRD spectrum, the $T_1 \leftarrow S_0$ carbonyl stretching region is obscured by intense $S_1 \leftarrow S_0$ bands near the singlet origin. To suppress this interference, we plan to record the $T_1 \leftarrow S_0$ spectrum using polarization-dependent CRD spectroscopy.[31] This technique combines the high sensitivity of CRD detection with the triplet selectivity of magnetic rotation[32] spectroscopy.

Acknowledgment. Acknowledgement is made to the Donors of The Petroleum Research Fund (No. 42824-B6), administered by the American Chemical Society, for partial support of this research. We also gratefully acknowledge the National Science Foundation for an RUI grant (No. CHE-0517879) and the Camille and Henry Dreyfus Foundation, Inc., for a Henry Dreyfus Teacher-Scholar Award to S.D. We thank Daniel Stupca for technical assistance. Computational resources were generously provided by the iOpenShell center for computational studies of electronic structure and spectroscopy of open-shell and electronically excited species at the University of Southern California. We thank Anna Krylov and Kadir Diri at USC for very helpful discussions.

References and Notes

(1) (a) Hoffmann, N. *Chem. Rev.* **2008**, *108*, 1052. (b) Klessinger, M.; Michl, J. *Excited States and Photochemistry of Organic Molecules*; VCH Publishers, Inc.: New York, 1995. (c) Turro, N. J. *Modern Molecular Photochemistry*; University Science Books: Sausalito, CA, 1991.

(2) Pillsbury, N. R.; Choo, J.; Laane, J.; Drucker, S. *J. Phys. Chem. A* **2003**, *107*, 10648.

(3) Pillsbury, N. R.; Zwier, T. S.; Judge, R. H.; Drucker, S. *J. Phys. Chem. A* **2007**, *111*, 8357.

(4) Drucker, S.; Van Zanten, J. L.; Gagnon, N. D.; Gilles, E. J.; Pillsbury, N. R. *J. Mol. Struct.* **2004**, *692*, 1.

(5) Hoffelt, L. M.; Springer, M. G.; Drucker, S. *J. Chem. Phys.* **2008**, *128*, 104312.

(6) *Computational Photochemistry*; Olivucci, M., Ed.; Elsevier: Amsterdam, The Netherlands, 2005.

(7) Grimme, S.; Izgorodina, E. *Chem. Phys.* **2004**, *305*, 223.

(8) Rhee, Y. M.; Head-Gordon, M. *J. Phys. Chem. A* **2007**, *111*, 5314.

(9) Hellwig, A.; Grün, S. A.; Hättig, C. *Phys. Chem. Chem. Phys.* **2008**, *10*, 4119.

(10) Bokoreva, O. S.; Bataev, V. A.; Pupyshev, V. I.; Godunov, I. A. *Int. J. Quantum Chem.* **2008**, *108*, 2719.

(11) O'Keefe, A.; Deacon, D. A. G. *Rev. Sci. Instrum.* **1988**, *59*, 2544.

(12) Tomer, J. L.; Holtzclaw, K. W.; Pratt, D. W.; Spangler, L. H. *J. Chem. Phys.* **1988**, *88*, 1528.

(13) Cheatham, C. M.; Laane, J. *J. Chem. Phys.* **1991**, *94*, 7734.

(14) Gordon, R. D.; Park, W. K. C. *Can. J. Chem.* **1993**, *71*, 1672.

(15) Throughout this paper, we use the same molecule-fixed coordinate system as Back and Gordon (ref 16). In this coordinate system, the b_2 label indicates symmetric character with respect to reflection in the molecular plane and b_1 indicates antisymmetric character. Other workers (particularly Fortunato and Giorgini (ref 17)) use a convention in which these labels are reversed.

(16) Back, R. A.; Gordon, R. D. *J. Mol. Spectrosc.* **2000**, *204*, 85.

(17) Fortunato, B.; Giorgini, M. G. *J. Mol. Struct.* **1977**, *37*, 27.

(18) Cramer, C. *Computational Chemistry*, 2nd ed.; Wiley: West Sussex, England, 2004.

(19) Shao, Y.; et al. *Phys. Chem. Chem. Phys.* **2006**, *8*, 3172.

(20) Purvis, G. D.; Bartlett, R. J. *J. Chem. Phys.* **1982**, *76*, 1910.

(21) Becke, A. D. *Phys. Rev. A* **1988**, *38*, 3098.

(22) Lee, C.; Yang, W.; Parr, R. G. *Phys. Rev. B* **1988**, *37*, 785.

(23) In our calculation of 0−0 excitation energies, we followed the procedure of Grimme and Izgorodina (ref 7) almost exactly. The only notable departure is our use of the cc-pVTZ basis set to determine excited-state energies instead of the aug-cc-pVTZ basis set used in ref 7. The augmented basis set presented convergence problems in our calculations. However, our substitution of the unaugmented basis set is justified by the accurate performance (see Computational Results section) of the method when applied to the experimentally known $S_1(n,\pi^*) \leftarrow S_0$ 0−0 excitation energy of 4CPD.

(24) Hougen, J. *Can. J. Phys.* **1964**, *42*, 443.

(25) Turro, N. J. Ibid.; p 105.

(26) Most of the $S_1 \leftarrow S_0$ hot bands have sharp, narrow contours characteristic of *a*-type transitions; however, a few others shown in Figure 5 are broader and more diffuse than any of the assigned $T_1 \leftarrow S_0$ transitions. These broadbands are vibronically induced *a*- or *b*-type transitions belonging to the $S_1 \leftarrow S_0$ system.

(27) Alternative candidates for the 482.2 cm^{-1} band assignment are disfavored on the basis of symmetry considerations. An N_0^1 transition involving an a_1 mode would have a narrower band profile, such as that observed for the $T_1 \leftarrow S_0$ origin. A b_1 mode would give rise to a one-peak rather than two-peak profile, as observed for the 19_0^1 band. An a_2 mode presumably does not undergo sufficient vibronic interaction to make its N_0^1 detectable; this conclusion is based on the absence of a 14_0^1 transition in the $T_1 \leftarrow S_0$ spectrum. Such a transition is predicted at 239 + 7 = 246 cm^{-1}, on the basis of the observed 14_1^1 band position and the precisely known16 ν''_{14} gas-phase fundamental. No band was detected at 246 cm^{-1}, suggesting that modes of a_2 symmetry are not vibronically active in the $T_1 \leftarrow S_0$ spectrum.

(28) The analysis presented here cites changes in bond order within the conjugated system to explain observed increases in ring vibrational frequencies upon $n \rightarrow \pi^*$ excitation. The frequency increases can also be partially explained (ref 16) in terms of the torsional potentials about the non-conjugated C1−C2 and C2−C3 bonds. The staggered equilibrium conformation of the methylene hydrogens with respect to the carbonyl groups corresponds to a minimum in the single-bond torsional potential of the (n,π^*) states but a maximum in the ground-state torsional potential. This situation could contribute to increases in ring-bending and ring-twisting frequencies upon excitation, because both of these modes involve torsional motion about C1−C2 and C2−C3. This might also partially explain why

the ring-twisting frequency in the $S_1(n,\pi^*)$ excited state is different from that in $T_1(n,\pi^*)$; i.e., the methylene hydrogens could have different conformations in the two excited states, leading to different torsional potentials. However, we do not favor this explanation because it would predict the two ring-bending frequencies to be different as well, which is contrary to observation.

(29) Cheatham, C. M.; Laane, J. *J. Chem. Phys.* **1991**, *94*, 5394.

(30) Csaszar, P.; Csaszar, A.; Somogyi, A.; Dinya, Z.; Holly, S.; Gal, M.; Boggs, J. E. *Spectrochim. Acta* **1986**, *42A*, 473.

(31) Engeln, R.; Berden, G.; van den Berg, E.; Meijer, G. *J. Chem. Phys.* **1997**, *107*, 4458.

(32) Carroll, T. *Phys. Rev.* **1937**, *52*, 882.

JP9041364